High energy PIXE: New experimental K-shell ionization cross sections for silver and gold and comparison with theoretical values from ECPSSR/RECPSSR models

Mostafa Hazim, Charbel Koumeir, Arnaud Guertin, Vincent Métivier, Adnan Naja, Noel Servagent, Ferid Haddad

HIGH ENERGY PIXE: NEW EXPERIMENTAL K-SHELL IONIZATION CROSS SECTIONS FOR SILVER AND GOLD AND COMPARISON WITH THEORETICAL VALUES FROM ECPSSR/RECPSSR MODELS

HAZIM Mostafa [1, 2, 3], KOUMEIR Charbel [1, 2], GUERTIN Arnaud [2], METIVIER Vincent [2], NAJA Adnan [3], SERVAGENT Noël [2] and HADDAD Férid [1, 2]
[1]GIP ARRONAX, Nantes-France
[2]Laboratoire SUBATECH, IMT Atlantique, CNRS/IN2P3, Université de Nantes, Nantes-France
[3]LPM, EDST, Lebanese University, Tripoli, Lebanon

Received month date year, amended month date year, accepted month date year

In high energy PIXE, a high energy ion beam, up to several tens of MeV, is used to analyze heavy elements in a thick sample. The knowledge of the interaction cross-section with the atoms is essential to perform quantitative analysis. As measured data in this range of energy are scarce, an experimental campaign was conducted at the C70 cyclotron of the GIP ARRONAX to measure the K-X-ray production cross-sections for silver and gold with proton energies 30, 42, 54 and 68 MeV. The detector efficiency, the beam intensity, and the target thickness were measured accurately to produce precise data. To convert the K-X-ray production cross-sections into the K-shell ionization cross-sections, an average value of the K-shell fluorescence yield, calculated from a compilation of existing data, was used. The outcomes of the campaign are in good agreement with the few existing data and the theoretical prediction of the RECPSSR model.

1. INTRODUCTION

ARRONAX, acronym for «Accelerator for Research in Radiochemistry and Oncology at Nantes Atlantique», is a high energy cyclotron. It allows the acceleration of several types of particle beams: 68 MeV alpha particles, 15-35 MeV deuterons and 30-68 MeV protons [1]. An experimental platform was implemented on ARRONAX to perform non-destructive material analysis with X-ray emission induced by high energy beams (HEPIXE) [2, 3, 4]. The HEPIXE has already been used to analyze geological samples with 66 and 85 MeV protons [5] and art objects (old paintings and coins) with 68 MeV protons [6]. One of the benefits of HEPIXE is the significant increase of the K-lines X-ray production cross-sections for medium and heavy elements with a high energy proton beam. Then, the identification of these elements with their K-X rays is possible allowing the analysis in depth of thick samples particularly if the bulk composition is different from the composition of the surface [6]. The knowledge of K-shell ionization cross sections is necessary to perform quantitative analysis. Currently, experimental data available at high energy are scarce. Therefore, we started to measure the K-X-ray production cross-sections for Ag and Au elements like to complement databases and to validate theoretical models. The experiments were carried out using high energy proton beams varying between 30 MeV and 68 MeV. Our results were compared with the existing data and with theoretical models.

1.1. Modeling and experimental cross section data

The inner shell ionization process by incident charged particles is modeled by different theoretical approaches, namely the Plane Wave Born Approximation PWBA [7] and the ECPSSR [8]. The last one is an upgrade of the PWBA model by the incorporation of corrective effects. The ECPSSR accounts for the energy loss (E) of the incident particle, the Coulomb deflection (C) of the incident particle, the perturbed-stationary state (PSS) and the relativistic (R) effect of the inner shell electrons. In addition, the relativistic effect of high energy projectile can be included, the model becoming RECPSSR [9]. The ECPSSR/RECPSSR model calculations, presented below, were performed using the ISICS software [10]. Many experiments have been carried out for the K-X-ray production and K-shell ionization cross sections induced by low energy protons [11-20]. Several comparisons with the experimental data have shown that the ECPSSR is a successful model for the determination of the cross section by light ions in the MeV energy range [16-18].
The database used in the present work, for Ag and Au, relies on different compilations available at high energy in the literature [21-28]. In the case of silver (Fig .1), the scattering of the data, associated with large error bars (above 15 MeV), makes the comparison with the ECPSSR and RECPSSR models unrealistic. In the case of gold (Fig. 2), the data have large error bars for energy above than 20MeV. Thus, it is not possible to

distinguish the best model describing the data between ECPSSR and RECPSSR.

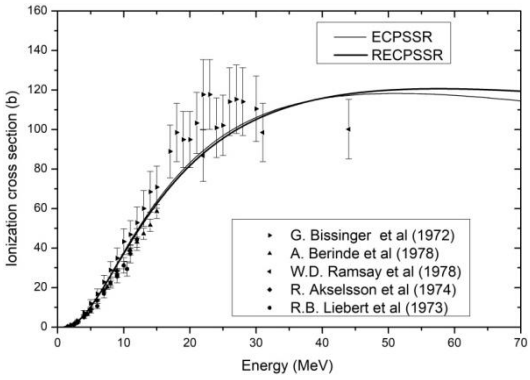

Figure 1 Experimental K-shell ionization cross section for silver with proton beam, compared to the ECPSSR/RECPSSR models.

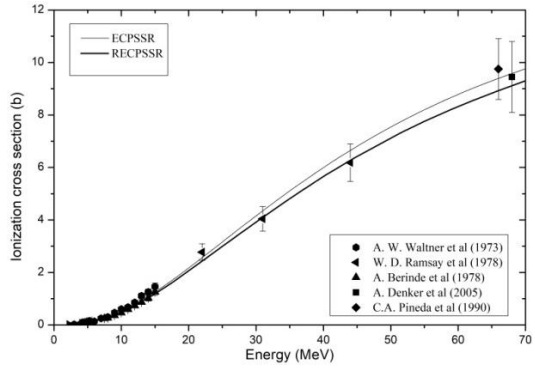

Figure 2 Experimental K-shell ionization cross section for gold with proton beam, compared to the ECPSSR/RECPSSR models.

2. MATERIALS AND METHODS

2.1. Experimental setup

The experimental setup is presented in the Fig. 3. After crossing a 75 µm Kapton window, the proton beam emerges in the air and passes through two Al collimator of 5 mm diameter. The target is located 30 cm downstream from the Kapton window. The beam energy loss in this air path is considered negligible. The X-rays, emitted from irradiated foils (Ag or Au), are detected normally to the target surface, placed at 45° with respect to the beam, by a shielded and cooled high purity germanium detector, HPGe (from Canberra, 50 mm² active area and 5 mm thick). The beam intensity is measured using a Faraday cup with a suitable electronics. The accuracy of the measured beam intensity is estimated around 1%. The beam intensity was adjusted around 100 pA to keep a reasonable dead time, below 4%, in the detector. The typical irradiation time was several tens of minutes to insure good statistics. The different foils, dimensions 25 × 25 mm^2, were of high purity (99.9%) and supplied by GoodFellow. The different targets were 10.1 ± 0.15 micrometer thick. Accurate values were obtained for each foil measuring their surface using a scanner (150 dpi) and their weight with a high precision scale (10^{-4} g).

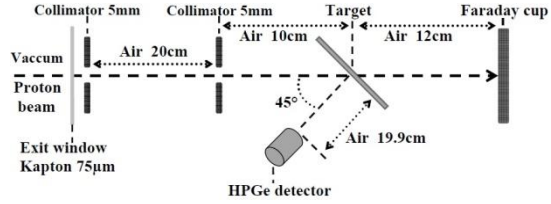

Figure 3 Schematic view of the experimental setup for cross section measurements

An efficiency model [29], optimized by the use of calibrated standard sources (^{241}Am, ^{109}Cd and ^{55}Fe), has been used to determine the detection efficiency for silver and gold K-X-rays. This model includes the intrinsic and the geometric efficiency of the detector. The errors on these efficiencies are below 3%.

2.2. X-ray spectrum

The table 1 presents the different allowed K_α and K_β transitions.

K_α	$K_{\alpha_1} = L_3 \rightarrow K$ $K_{\alpha_2} = L_2 \rightarrow K$	
K_β	K_{β_1}'	$K_{\beta_1} = M_3 \rightarrow K$ $K_{\beta_3} = M_2 \rightarrow K$ $K_{\beta_5} = M_{4,5} \rightarrow K$
	K_{β_2}'	$K_{\beta_2} = N_{2,3} \rightarrow K$ $K_{\beta_4} = N_{4,5} \rightarrow K$

Tableau 1 K_α and K_β transitions

The graph (Fig. 4) shows two X-ray spectra obtained from irradiation of respectively Ag and Au targets with a 30 MeV proton beam. In the case of silver, the detected transitions are K_α, $K_{\beta 1}'$ and $K_{\beta 2}'$, and in case of gold, the detected transitions are $K_{\alpha 1}$, $K_{\alpha 2}$, $K_{\beta 1}'$ and $K_{\beta 2}'$, (Fig. 5). The different transitions listed in table 1 cannot be distinguished in the detected spectra due to the detector energy resolution.

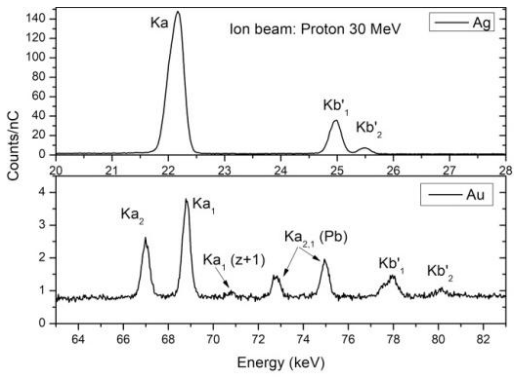

Figure 4: X-ray spectra obtained from the bombardment, with 30 MeV protons, of a silver target (top) and a gold target (bottom). Subscript a and b means alpha and beta respectively.

In the gold spectrum, the small peak, $K_{\alpha 1}$ (Z+1), comes from the internal conversion of the residual atoms called "nuclear satellites" produced by the (p, xn) nuclear reactions [22]. The position of the $K_{\alpha 2}$ (Z+1) peak is the same as the gold Kα1 peak. The $K_{\alpha 2}$ (Z+1) is at the same or lower level than the background, and its contribution to the area of the gold Kα1 peak is negligible. In the silver spectra, the satellites were not visible. The 72.8 keV and 74.97 keV peaks correspond to the K-X-rays of lead atoms contained in the detector shield. The peak area of a given transition was calculated by the subtraction of a linear background from the peak integral.

2.3. K-X-rays production cross section

The K_i-X-rays production cross-section formula is independent of the fluorescence yield ω_z and the intensity of a given transition. This K_i-X-rays production cross section is given by

$$\sigma_P(K_i) = \frac{N_X(K_i) \times \frac{\mu}{\rho}(K_i) \times M \times \cos(45)}{N_P \times N_A \times \varepsilon_{tot}(K_i) \times \left(1 - e^{-\frac{\mu}{\rho}(K_i) \times \rho \times d)}\right)} \quad (1)$$

Where Np and $N_X(K_i)$ are the number of incident protons and the detected number of K_i-X-rays photons, respectively, N_A is the Avogadro constant, M is the mass number of the target, μ/ρ is the photon mass attenuation coefficient at the energy of interest, ρ is the target density and ε is the detector efficiency at this energy. The error associated to the cross section measurement contains the errors on the particles beam number, the detector efficiency, the target thickness and the uncertainty on the number of X-rays. The total K X-ray production cross section $\sigma_P^T(K)$ is given by the sum of all K_i cross sections:

$$\sigma_P^T(K) = \sum_i \sigma_P(K_i) \quad (2)$$

2.4. K-shell ionization cross section

The K-shell ionization cross section $\sigma_I(K)$ is equal to the K-X-rays $\sigma_P^T(K)$ production cross section divided by the fluorescence yield ω_K:

$$\sigma_I(K) = \frac{\sigma_P^T(K)}{\omega_K} \quad (3)$$

This cross section is used to compare with the theoretical one given by the models.

The fluorescence yields were calculated by the weighted average [30] value of experimental data and are summarized in Table 2. The weighted average value and its associated standard deviation are given respectively by the equation (4) and (5):

$$\overline{\omega}_{K_W} = \left(\sum_{i=1}^{N}\left(\frac{1}{\Delta\omega_i}\right)^2\right)^{-1} \sum_{i=1}^{N}\left(\frac{\omega_{Ki}}{(\Delta\omega_i)^2}\right) \quad (4)$$

$$\Delta\overline{\omega}_{K_W} = \sqrt{\left(\sum_{i=1}^{N}\left(\frac{1}{\Delta\omega_i}\right)^2\right)^{-1} \sum_{i=1}^{N}\left(\frac{(\omega_{Ki} - \overline{\omega}_K)^2}{(\Delta\omega_i)^2}\right)} \quad (5)$$

Target	ω_{Ki}	Ref	$\overline{\omega}_K$	$\overline{\omega}_{K_W}$
Ag	0.843 ± 0.046	[32]	0.835	0.833 ± 0.011
	0.856 ± 0.025	[33]		
	0.857 ± 0.034	[34]		
	0.861 ± 0.072	[35]		
	0.826 ± 0.005	[36]		
	0.836 ± 0.04	[37]		
	0.829 ± 0.038	[38]		
	0.843 ± 0.047	[39]		
	0.818 ± 0.018	[40]		
	0.815 ± 0.041	[41]		
	0.827 ± 0.066	[42]		
	0.830 ± 0.026	[43]		
	0.821 ± 0.032	[44]		
	0.834 ± 0.01	[45]		
Au	0.959 ± 0.014	[43]	0.963	0.959 ± 0.004
	0.967 ± 0.083	[46]		

Table 2 Summary of the experimental fluorescence yield $\boldsymbol{\omega_{Ki}}$, average value $\overline{\boldsymbol{\omega}}_{\mathbf{K}}$ and weighted average value $\overline{\boldsymbol{\omega}}_{\mathbf{K_W}}$ for Silver and gold.

3. RESULTS

3.1. K-X-ray production cross section

The K_α, $K_{\beta 1'}$, and $K_{\beta 2'}$ X-ray production cross sections for silver, obtained for four different proton beam energies, are given in Table 3.

Energy (MeV)	$\sigma_P(K_\alpha)$ *(barn)*	$\sigma_P(K_{\beta}'_1)$ *(barn)*	$\sigma_P(K_{\beta}'_2)$ *(barn)*
30	74.8 ± 2.9	13.0 ± 0.8	2.3 ± 0.15
42	81.7 ± 3.0	13.8 ± 0.7	2.5 ± 0.14
54	83.5 ± 3.2	14.2 ± 0.8	2.5 ± 0.15

68	82.6 ± 3.2	14.3 ±0.8	2.5 ± 0.15

Table 3: The K_{α}, $K_{\beta 1'}$, and $K_{\beta 2'}$ X-ray production cross sections for silver for different beam energies.

The error associated to the X-ray production cross section for the main peak, K_{α} "$\sigma_P(K_{\alpha})$", is less than 4%, whereas it is less than 6 % for the other peaks, $K_{\beta 1'}$ "$\sigma_P(K_{\beta}{}'_1)$" and $K_{\beta 2'}$ "$\sigma_P(K_{\beta}{}'_2)$".
Table 4 presents the $K_{\alpha 1}$, $K_{\alpha 2}$, $K_{\beta 1'}$, and $K_{\beta 2'}$ X-ray production cross sections for gold obtained for four different proton beam energies.

Energy (MeV)	$\sigma_P(K_{\alpha_1})$ *(barn)*	$\sigma_P(K_{\alpha_2})$ *(barn)*	$\sigma_P(K_{\beta}{}'_1)$ *(barn)*	$\sigma_P(K_{\beta}{}'_2)$ *(barn)*
30	1.76 ± 0.05	1.04 ± 0.03	0.57 ± 0.03	0.17 ± 0.02
42	2.74 ± 0.07	1.63 ± 0.05	0.87 ± 0.04	0.27 ± 0.03
54	3.57 ± 0.10	2.13 ± 0.07	1.21 ± 0.06	0.31 ± 0.04
68	4.26 ±0.13	2.53 ± 0.08	1.47 ±0.07	0.34 ± 0.04

Table 4: The $K_{\alpha 1}$, $K_{\alpha 2}$, $K_{\beta 1'}$, and $K_{\beta 2'}$ X-ray production cross sections for gold for the different beam energies.

The experimental errors are less than 3% for $K_{\alpha 1}$ and $K_{\alpha 2}$, less than 6% for $K_{\beta 1'}$ and close to 12% for $K_{\beta 2'}$.
Table 5 presents the total K-X-ray production cross sections $\sigma_P^T(K)$ for silver and gold obtained for the four different proton beam energies (calculated according to equation 2). The error on the K-X-ray production cross section varies between 3.7 and 4.4 %.

Energy (MeV)	$\sigma_P^T(K)$ *(barn)*	
	Ag	Au
30	90.1 ± 3.9	3.53 ± 0.14
42	98 ± 3.8	5.52 ± 0.18
54	100.2 ± 4.1	7.22 ± 0.27
68	99.5 ± 4.1	8.60 ± 0.32

Table 5: K-X-ray production cross sections for silver and gold for the different beam energies.

3.2. K-shell ionization cross section

To compare the results with values extracted from theoretical models, the K-shell ionization cross sections have to be determined according to the equation (3).

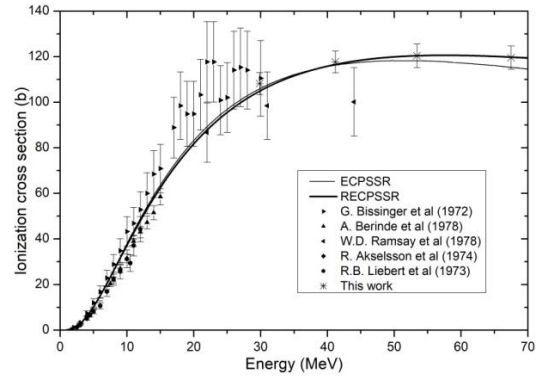

Figure 5 Experimental ionization cross sections as a function of the proton beam energy for silver compared with the ECPSSR/RECPSSR models. The stars correspond to the results presented in this work.

Fig. 5 presents our new experimental values for K-shell ionization cross sections for silver (stars) as a function of the proton beam energy, compared to the existing data and the ECPSSR/RECPSSR models (lines).
These points cover a common region (30 MeV-42 MeV) with those of W. D. Ramsay [23] and G. Bissinger [21]. The difference with our points varies between 2% and 12%. Our new data point at 30 MeV is in agreement with the existing one [21]. Our experimental data are in better agreement with the theoretical models than other experimental ones above 30 MeV. The two model calculations are in agreement with our data points considering the associated error bars.

Fig. 6 presents our new data points for K-shell ionization cross section for gold (stars) as a function of the proton beam energy, compared to the existing data (between 1973 and 2005) and the ECPSSR/RECPSSR models.

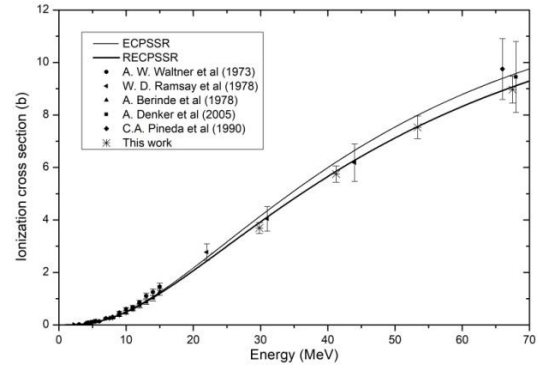

Figure 6 Experimental ionization cross sections as a function of the proton beam energy for gold compared with the ECPSSR/RECPSSR models. The stars correspond to the results presented in this work.

We found a 5% deviation with the data points published by A. Denker [28] at 68 MeV and a 9% difference from the data point of C.A. Pineda [27] at 66 MeV. These values are compatible with each other within the error bars. The new points, at 30 and 40MeV, are in good agreement with the trend of the points given by W. D. Ramsay [23].
Our points have error bars smaller than other existing data, which helps to compare with the two close models ECPSSR and RECPSSR: they are in the same trend as the ECPSSR model, but in better agreement with the RECPSSR model.

4. CONCLUSION

A new set of data for proton induced K-X-ray production cross sections have been obtained at the high energy cyclotron ARRONAX in Nantes (France)
These new measurements were performed at 30, 42, 54 and 68 MeV for silver and gold with errors ranging between 4 and 7 %. The weighted average values of the experimental fluorescence yields have been used to convert K-X-ray cross sections into K-Shell ionization cross sections. These latter are in good agreement with the trend of low energy measurements and within the error bars with the scarce existing high energy experimental data. As expected, the RECPSSR model which includes relativistic effects for the projectile seems better reproducing these new experimental data than the ECPSSR model.
The K-shell ionization cross section measurements now need to be extended to other medium and heavy elements, which is necessary to complete the database and to validate the theoretical models that can be used for HEPIXE quantitative analysis.

ACKNOWLEGMENTS

The cyclotron Arronax is supported by CNRS, Inserm, INCa, the Nantes University, the Regional Council of Pays de la Loire, local authorities, the French government and the European Union. This project is supported by an ANR grant called “Investissements d’Avenir”, Equipex Arronax-Plus (ANR-11-EQPX-0004), Labex IRON (ANR-11-LABX-18-01) and ISITE NExT (ANR-16-IDEX-0007).

References

1. F. Haddad, L. Ferrer, A. Guertin, T. Carlier, N. Michel, J. Barbet, J-F. Chatal, a high-energy and high-intensity cyclotron for nuclear medicine, European Journal of Nuclear Medicine and Molecular Imaging, (2008), 35, 1377-1387.
2. C. Koumeir, F. haddad, V. Metivier, N. Servagent, X. de la Bernardie, E. Garrido, D. Ragheb,.al, High Energy PIXE at the ARRONAX Facility for Multi Elemental Analysis of Thick Samples, AIP Conference Proceedings (2011), 1412, 105.
3. D. Ragheb, C. Koumeir, V. Métivier, J. Gaudillot, A. Guertin, F. Haddad, N. Michel, N. Servagent, Development of a PIXE method at high energy with the ARRONAX cyclotron, Journal of Radioanalytical and Nuclear Chemistry, (2014), 302, 895-901.
4. A. Subercaze C. Koumeir, V. Métivier, N. Servagent, A. Guertin, F. Haddad, High energy PIXE: A tool to characterize multi-layer thick samples, Nuclear Instruments and Methods in Physics Research B, (2018), 417, 41-45.
5. C. A. Pineda, M. Peisach, Prompt analysis of rare earths by high-energy PIXE, Journal of Radioanalytical and Nuclear Chemistry, (1991), 151, 387-396.
6. A. Denker, W. Bohne, J. Opitz-Coutureau, J. Rauschenberg, J. Röhrich, E. Strub, Influence of corrosion layers on quantitative analysis, Nuclear Instruments and Methods in Physics Research B, (2005), 239, 65-70.
7. E. Merzbacher and H. Lewis, Encyclopedia of physics, (1958), 34, 166.
8. W. Brandt and G. lapicki, Energy-loss effect in inner-shell coulomb ionization by heavy charged particles, Phys. Rev. A, (1981), 23, 1717.
9. G. Lapicki, Scaling of analytical cross sections for K-shell ionization by nonrelativistic protons to cross sections by protons at relativistic velocities, Journal of Physics B, (2008), 41, 115201.
10. Sam J. Cipolla, An improved version of ISICS: a program for calculating K-, L- and M-shell cross sections from PWBA and ECPSSR theory using a personal computer, Computer Physics Communications, (2007), 176, 157-159.
11. C. H. Rutledge and R. L. Watson, Cross sections for K-Shell ionization by ^{1}H, ^{2}H, ^{3}He and ^{4}He ion impact, Atomic Data and Nuclear Data Tables, (1973), 12, 195-216.
12. E. Lægsgaard, J. U. Andersen, F. Hogedal, Accurate determination of cross sections for K-shell ionization by proton impact, Nuclear Instruments and Methods, (1980), 169, 293-300.
13. H. Paul and J. Sacher, Fitted empirical reference cross sections for K-Shell ionization by protons, Atomic Data and Nuclear Data Tables, (1989), 42, 105-156.
14. G. Lapicki, cross sections for K- Shell X-ray production by Hydrogen and helium ions in Elements grom Beryllium to uranium, Journal of Physical and Chemical Refernce Data, (1989), 18, 111-218.
15. H. Janžekovič, Ž. Šmit, M. Budnar, A. Mühleisen, M. Ravnikar, V. Ramšak, P. Pelicon, K shell ionization cross sections of Au, Pb and Bi induced by low energy proton impact, Nuclear Instruments and Methods in Physics Research B, (1995), 100, 10-16
16. S. Ouziane, A. Amokrane, M. Zilabdi, Experimental measurement of X-ray production cross-section by proton of energies between 1 and 2,3 MeV and comparison with theoretical predictions of PWBA and ECPSSR models, Nuclear Instruments and Methods in Physics Research B, (2000), 161-163, 141-144.
17. A. Kahoul, M. Nekkab, B. Deghfel, Empirical K-shell ionization cross-sections of elements from $_{4}$Be to $_{92}$U by proton impact, Nuclear Instruments and Methods in Physics Research B, (2008), 266, 4969-4975.

18. J. Reyes-Herrera and J.Miranda, K X-ray production by 3–4MeV proton impact on selected lanthanoids, Radiation Physics and Chemistry, (2010), 79, 1013–1017.
19. X. Zhou, Y. Zhao, R. Cheng, Y. Wang, Y. Lei, X. Wang, Y. Sun, K and L-shell X-ray production cross sections for 50-250 keV proton impact on elements with Z = 26-30, Nuclear Instruments and Methods in Physics Research B, (2013), 299, 61-67.
20. E. Batyrbekov, I. Gorlachev, I. Ivanov, A. Platov, K-, L- and M- shell X-ray production cross sections by 1-1.3 MeV protons, Nuclear Instruments and Methods in Physics Research B, (2014), 325, 84-88.
21. G. A. Bissinger, S. M. Shafroth, and A. W. Waltner, Yields of K and L X Rays Arising from 2-30 MeV-Proton Bombardment of Ag, Phys. Rev. A, (1972), 5, 2046.
22. A. Berinde, C. Deberth, I. Neamu, C. Protop, N. Scintei, V. Zoran, M. Dost and S. Rohl, Relativistic effects in K-shell ionisation by 7-15 MeV proton bombardment on heavy elements, Journal of Physics B: Atomic and Molecular Physics, (1978), 11, 2875.
23. W. D. Ramsay, M.S.A.L. Al-Ghazi, J. Birchall, J.S.C. McKee, Atomic K-shell ionization induced by 20–50 MeV protons, Physics Letters A, (1978), 69, 258-260.
24. R. Akselsson and T. B. Johansson, X-ray production by 1.5-11 MeV protons, Zeitschrift für Physik, (1974), 266, 245-255.
25. R. B. Liebert, R. B. Liebert, T. Zabel, D. Miljanić, H. Larson, V. Valković, and G. C. Phillips, X-Ray Production by Protons of 2.5-12 MeV Energy, Phys. Rev. A, (1973), 8, 2336-2341.
26. S. M. Shafroth, G. A. Bissinger, A.w. Waltner, A Study of K and L Shell Ionization Arising From 2-30 MeV Proton Bombardment of Ag, Proceedings of International Conference on Inner Shell Ionization Phenomena, Atlanta (1972), 2, 1057-1068.
27. C. A. Pineda and M. Peisach, Prompt analysis of heavy elements by high-energy-induced (p, X) reactions, Nuclear Instruments and Methods in Physics Research A, (1990), 299, 618-623.
28. A. Denker, W. Bohne, J. L. Campbell, P. Heide, T. Hopman, J. A. Maxwell, J. Opitz-Coutureau, J. Rauschenberg, J. Röhrich, E. Strub, High-energy PIXE using very energetic protons: quantitative analysis and cross-sections, X-Ray Spectrometry, (2005), 34, 376-380.
29. Y. Selim and M. I. Abass, Direct calculation of the total efficiency of cylindrical scintillation detectors for extended circular sources, Radiation Physics and Chemistry, (1996), 48, 23-27.
30. A. Kahoul, V. Aylikci, N. Kup Aylikci, E. Cengiz, G. Apaydın, Updated database and new empirical values for K-shell fluorescence yields, Radiation Physics and Chemistry, (2012), 81, 713-727.
31. I. A. Al-Nasr, I. J. Jabr, K. A. Al-Saleh, N. S. Saleh, Measurement of Ka cross sections and fluorescence yields for elements in the range 42<Z<57 using radioisotope X-ray fluorescence, Appl. Phys. A, (1987), 43, 71-73.
32. M. L. Garg, Devinder Mehta, Sudhir Kumar, P. C. Mangal, P. N. Trehan, Energy dependence of photon-induced Ka and Kb X-ray fluorescence cross sections for some elements with 20<Z<56, X-Ray Spectrometry, (1985), 14, 165-169.
33. S. K. Arora, K. L. Allawadhi, B. S. Sood, Measurement of K-shell fluorescence yields in elements 28<Z<53, Physica B+C, (1981), 111, 71-75.
34. C. Bhan, S. N. Chaturvedi, N. Nath, Measurement of K X-ray fluorescence cross-sections, X-Ray Spectrometry, (1981), 10, 128-130.
35. M. Takiue and H. Ishikawa, K- fluorescence yields of Ag and In, Nuclear Instruments and Methods, (1980), 173, 391-394.
36. K. M. Balakrishna, N. Govinda Nayak, N. Lingappa and K. Siddappa, K fluorescence yield measurements in rare earth and heavy elements, Journal of Physics B: Atomic, Molecular and Optical Physics, (1994), 27, 715-720.
37. R. Durak and Y. Özdemır, Measurement of K-shell fluorescence cross-sections and yields of 14 elements in the atomic number range $25 \leqslant Z \leqslant 47$ using photoionization, Radiation Physics and Chemistry, (2001), 61, 19-25.
38. Ö. Şimşek, M. Ertugrul, D. Karagöz, G. Budak, A. Karabulut, S. Yılmaz, O. Doğan, Ü. Turgut, Ö Söğüt, R. Polat, A. Gürol, K shell fluorescence yields for elements with $33 < Z < 53$ using 59.5 photons, Radiation Physics and Chemistry, (2002), 65, 27-31.
39. Ö. Şimşek, S. Yılmaz, D. Karagöz, M. Ertugrul, Measurement of K shell fluorescence cross sections and K-shell fluorescence yields for the atomic region $22 \leq Z \leq 64$ by 59.5 keV photons, Journal of Radioanalytical and Nuclear Chemistry, (2002), 253, 143-147.
40. S. Seven, A method for the determination of K shell fluorescence yields using photoionization, Journal of Quantitative Spectroscopy and Radiative Transfer, (2002), 74, 69-74.
41. M. Ertugrul, A. Karabulut, G. Budak, Measurement of the K shell absorption jump factor of some elements, Radiation Physics and Chemistry, (2002), 64, 1-3.
42. S. B. Gudennavar, N.M. Badiger, S.R. Thontadarya, B. Hanumaiah, K-shell fluorescence parameters of medium-Z elements, Radiation Physics and Chemistry, (2003), 68, 721-726.
43. T. Yashoda, S. Krishnaveni, Ramakrishna Gowda, Measurements of K shell fluorescence yields for the elements in the range $22 \leq Z \leq 52$ excited by 14.4 and 122 keV photons, Nuclear Instruments and Methods in Physics Research B, (2005), 240, 607-611.
44. A. S. Bennal and N. M. Badiger, Measurement of K shell absorption and fluorescence parameters for the elements Mo, Ag, Cd, In and Sn using a weak gamma source, Journal of Physics B: Atomic, Molecular and Optical Physics, (2007), 40, 2189-2199.
45. G. Apaydin and E. Tiraşoğlu, Measurements of K shell X-ray production cross sections and fluorescence yields of elements in the atomic number range 65< Z< 92 at 123.6 keV, Nuclear Instruments and Methods in Physics Research B, (2006), 246, 303-308.

Table 1

K_α	$K_{\alpha_1} = L_3 \rightarrow K$ $K_{\alpha_2} = L_2 \rightarrow K$	
K_β	$K_{\beta_1}{}'$	$K_{\beta_1} = M_3 \rightarrow K$ $K_{\beta_3} = M_2 \rightarrow K$ $K_{\beta_5} = M_{4,5} \rightarrow K$
	$K_{\beta_2}{}'$	$K_{\beta_2} = N_{2,3} \rightarrow K$ $K_{\beta_4} = N_{4,5} \rightarrow K$

Table 2

Target	ω_{Ki}	Ref	$\bar{\omega}_K$	$\overline{\omega}_{K_W}$
Ag	0.843 ± 0.046 0.856 ± 0.025 0.857 ± 0.034 0.861 ± 0.072 0.826 ± 0.005 0.836 ± 0.04 0.829 ± 0.038 0.843 ± 0.047 0.818 ± 0.018 0.815 ± 0.041 0.827 ± 0.066 0.830 ± 0.026 0.821 ± 0.032 0.834 ± 0.01	[32] [33] [34] [35] [36] [37] [38] [39] [40] [41] [42] [43] [44] [45]	0.835	0.833 ± 0.011
Au	0.959 ± 0.014 0.967 ± 0.083	[43] [46]	0.963	0.959 ± 0.004

Table 3

Energy (MeV)	$\sigma_P(K_\alpha)$ ***(barn)***	$\sigma_P(K_{\beta'1})$ ***(barn)***	$\sigma_P(K_{\beta'2})$ ***(barn)***
30	74.8 ± 2.9	13.0 ± 0.8	2.3 ± 0.15
42	81.7 ± 3.0	13.8 ± 0.7	2.5 ± 0.14
54	83.5 ± 3.2	14.2 ± 0.8	2.5 ± 0.15
68	82.6 ± 3.2	14.3 ±0.8	2.5 ± 0.15

Table 4

Energy (MeV)	$\sigma_P(K_{\alpha 1})$ ***(barn)***	$\sigma_P(K_{\alpha 2})$ ***(barn)***	$\sigma_P(K_{\beta' 1})$ ***(barn)***	$\sigma_P(K_{\beta' 2})$ ***(barn)***
30	1.76 ± 0.05	1.04 ± 0.03	0.57 ± 0.03	0.17 ± 0.02
42	2.74 ± 0.07	1.63 ± 0.05	0.87 ± 0.04	0.27 ± 0.03
54	3.57 ± 0.10	2.13 ± 0.07	1.21 ± 0.06	0.31 ± 0.04
68	4.26 ±0.13	2.53 ± 0.08	1.47 ±0.07	0.34 ± 0.04

Table 5

Energy (MeV)	$\sigma_P^T(K)$ ***(barn)***	
	Ag	Au
30	90.1 ± 3.9	3.53 ± 0.14
42	98 ± 3.8	5.52 ± 0.18
54	100.2 ± 4.1	7.22 ± 0.27
68	99.5 ± 4.1	8.60 ± 0.32

Figure1

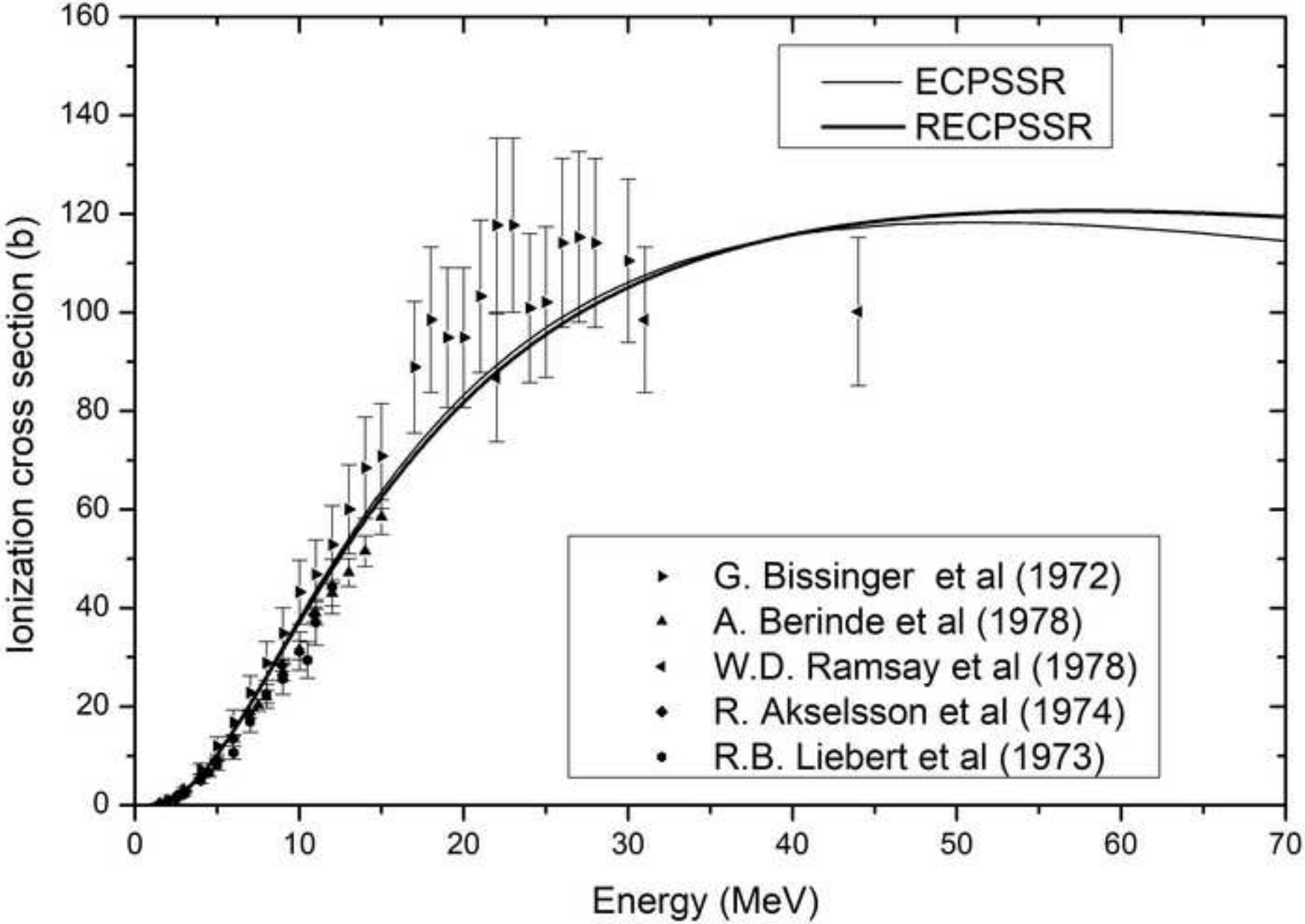
ECPSSR
RECPSSR
G. Bissinger et al (1972)
A. Berinde et al (1978)
W.D. Ramsay et al (1978)
R. Akselsson et al (1974)
R.B. Liebert et al (1973)
Ionization cross section (b)
Energy (MeV)
0
20
40
60
80
100
120
140
160
0
10
20
30
40
50
60
70

Figure2

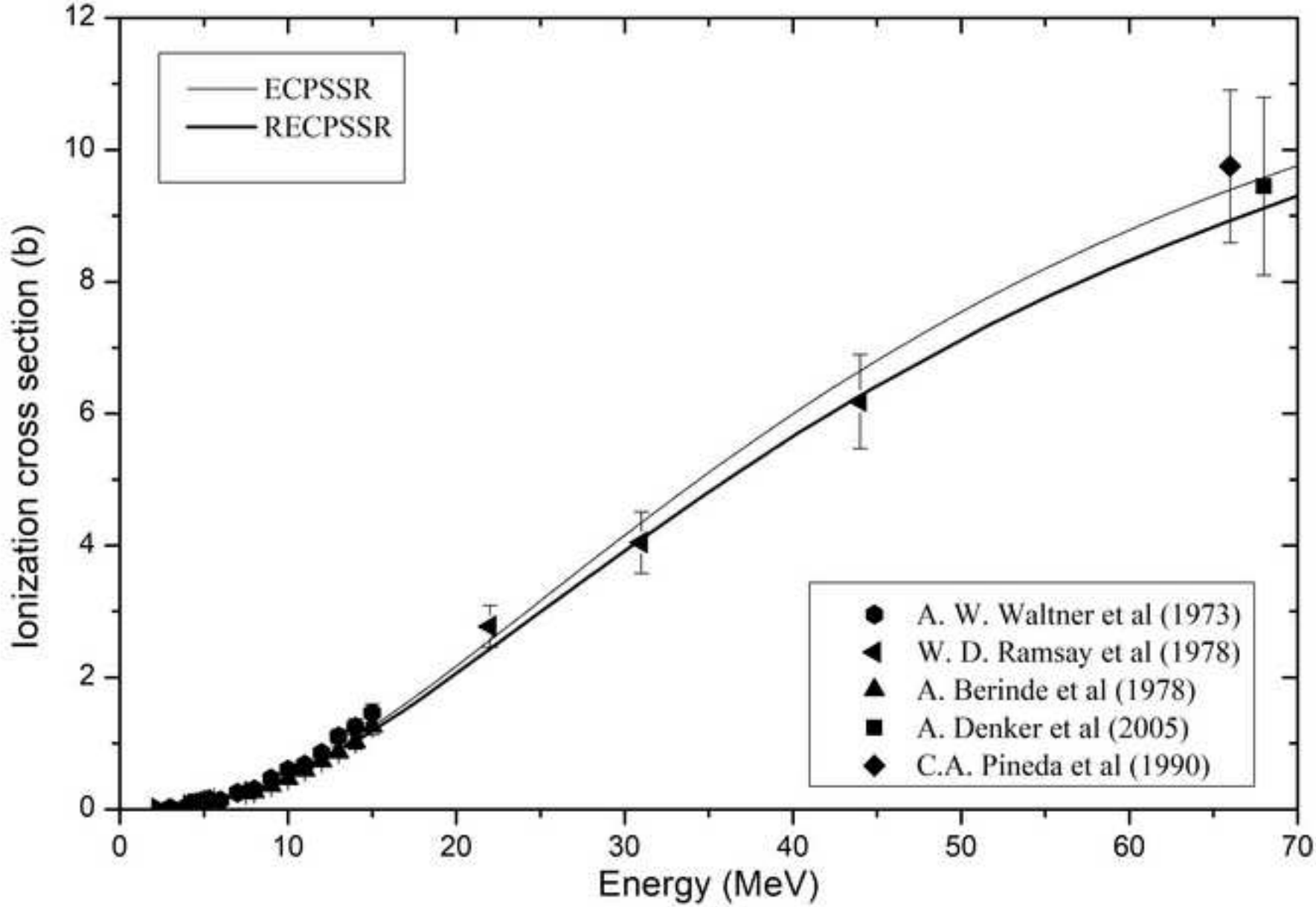
ECPSSR
RECPSSR
A. W. Waltner et al (1973)
W. D. Ramsay et al (1978)
A. Berinde et al (1978)
A. Denker et al (2005)
C.A. Pineda et al (1990)
Ionization cross section (b)
Energy (MeV)
0
2
4
6
8
10
12
0
10
20
30
40
50
60
70

Figure3

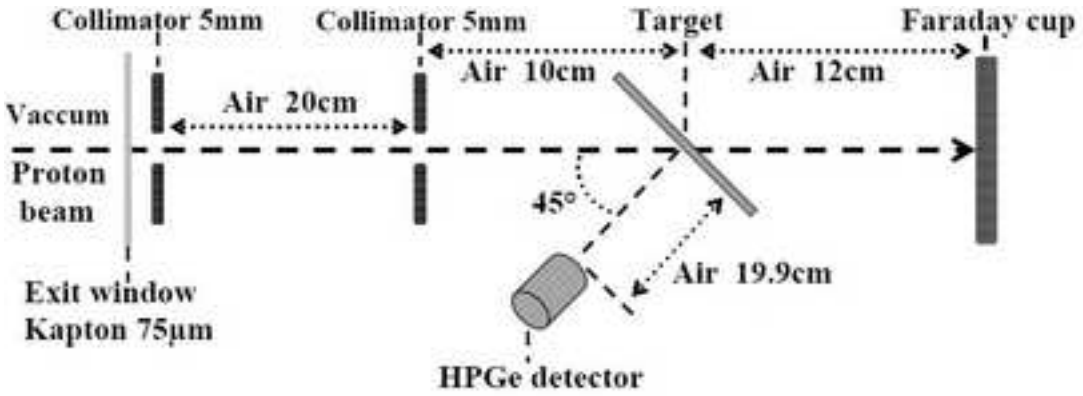
Collimator 5mm
Collimator 5mm
Target
Faraday cup
Air 10cm
Air 12cm
Air 20cm
Vaccum
Proton beam
45°
Air 19.9cm
Exit window
Kapton 75μm
HPGe detector

Figure4

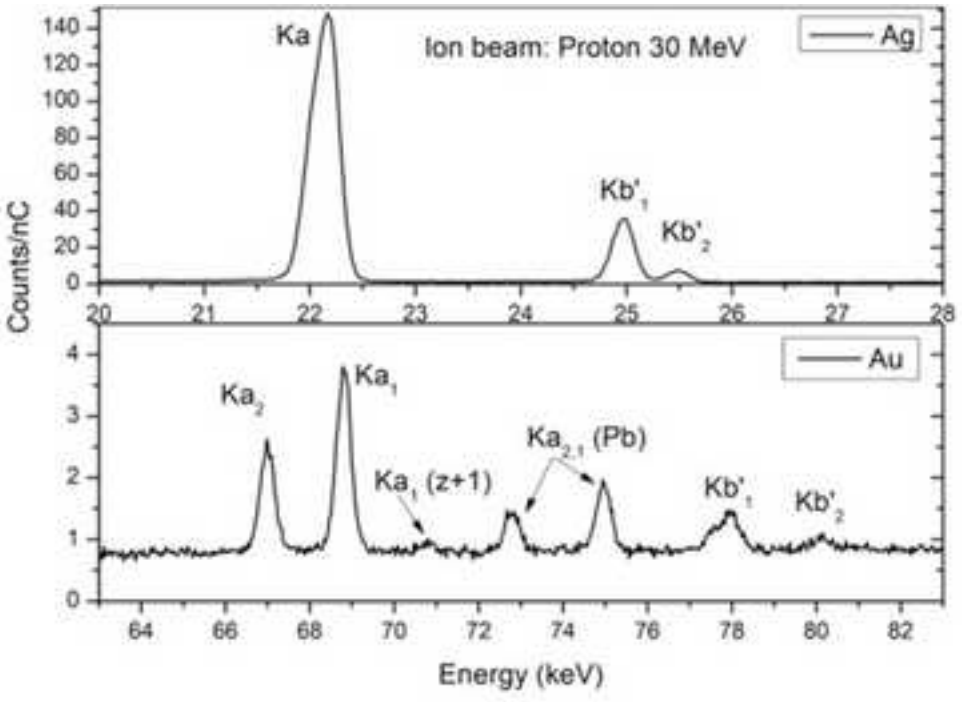
Ka
Ion beam: Proton 30 MeV
Ag
Kb'1
Kb'2
Counts/nC
Au
Ka2
Ka1
Ka1 (z+1)
Ka2,1 (Pb)
Kb'1
Kb'2
Energy (keV)

Figure5

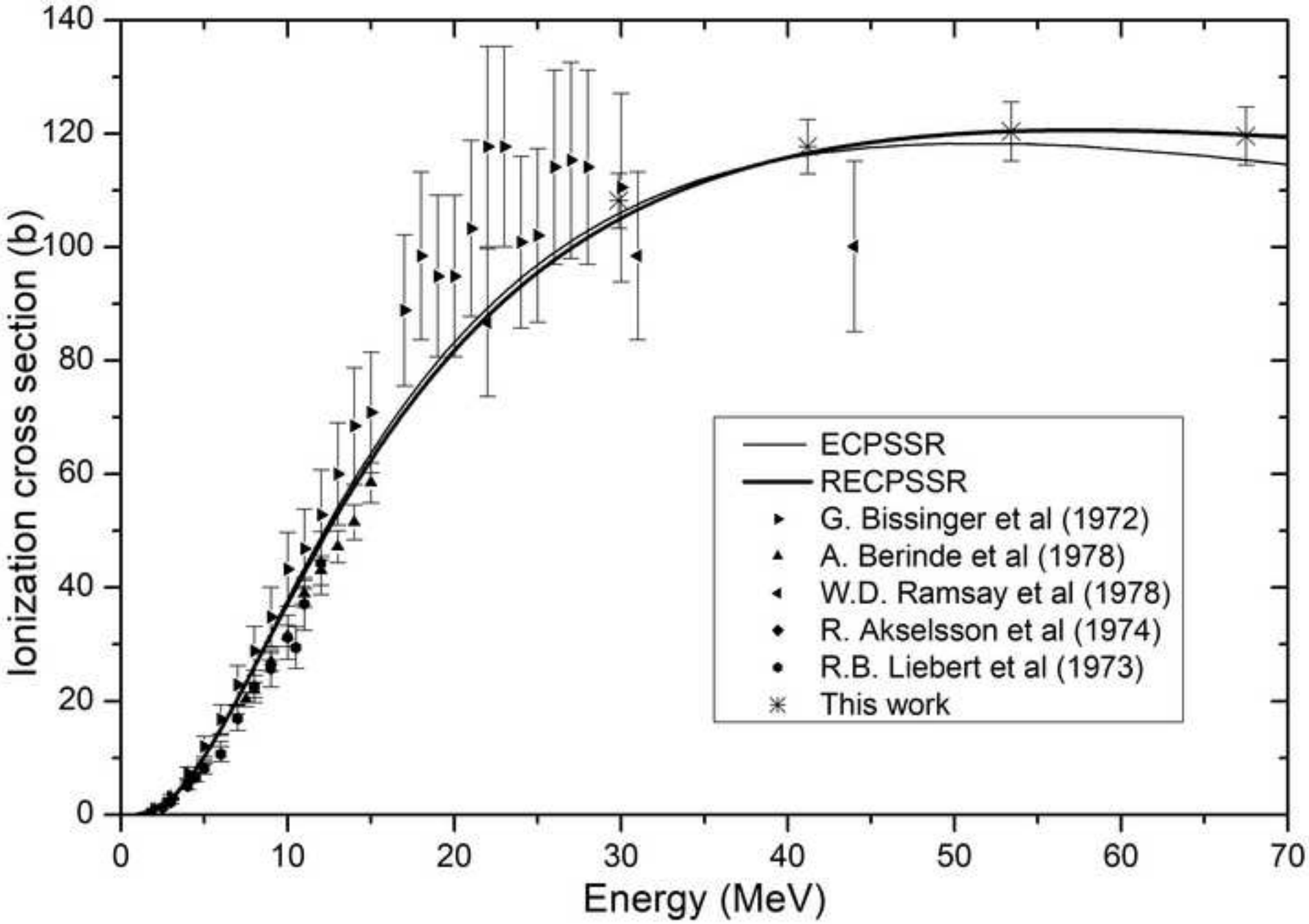
Ionization cross section (b)
Energy (MeV)
0
20
40
60
80
100
120
140
0
10
20
30
40
50
60
70
ECPSSR
RECPSSR
G. Bissinger et al (1972)
A. Berinde et al (1978)
W.D. Ramsay et al (1978)
R. Akselsson et al (1974)
R.B. Liebert et al (1973)
This work

Figure6

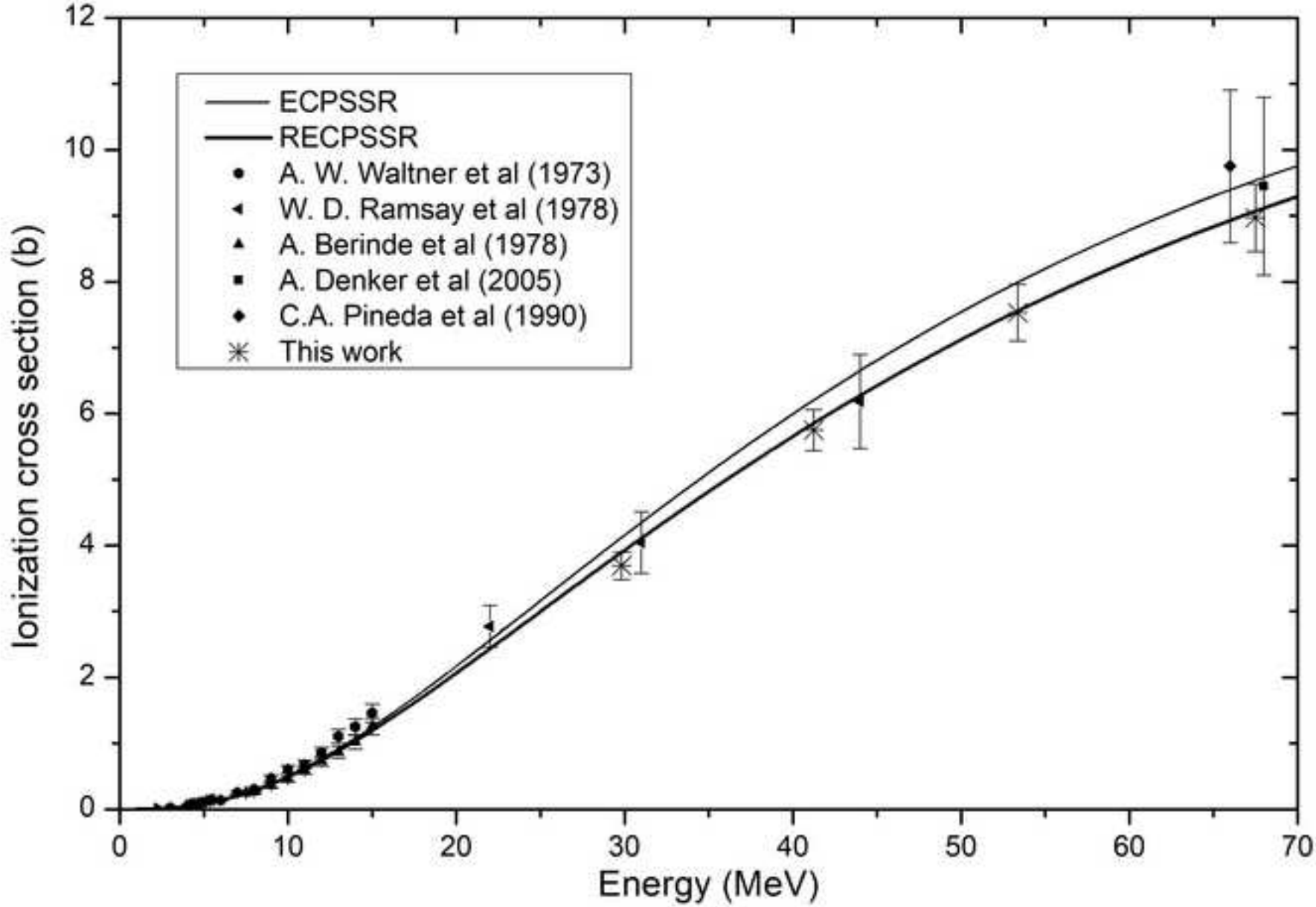
ECPSSR
RECPSSR
A. W. Waltner et al (1973)
W. D. Ramsay et al (1978)
A. Berinde et al (1978)
A. Denker et al (2005)
C.A. Pineda et al (1990)
This work
Ionization cross section (b)
Energy (MeV)
0
2
4
6
8
10
12
0
10
20
30
40
50
60
70